River, Coastal and Estuarine Morphodynamics: RCEM2011

Modelling the formation of transverse sand bars: application to Duck beach, USA

Francesca RIBAS
Department of Applied Physics
Universitat Politècnica de Catalunya
Edifici C3, Campus del Baix Llobregat, c/ Esteve Terradas 5, 08860 Castelldefels, Spain

Huib E. DE SWART
Institute for Marine and Atmospheric research Utrecht
Utrecht University
Princetonplein 5, 3584CC Utrecht, the Netherlands

Daniel CALVETE, Albert FALQUES
Department of Applied Physics
Universitat Politècnica de Catalunya
Edifici B4/B5, Campus Nord, c/ Jordi Girona 1-3, 08034 Barcelona, Spain

ABSTRACT: A morphodynamic model has been applied to explain the formation of transverse sand bars at Duck beach, USA. The model describes the feedback between waves, rollers, depth-averaged currents and bed evolution, so that self-organized processes can develop. The wave and bathymetric conditions measured at Duck are used to perform the simulations. Subsequently, modelled bar characteristics are compared with those observed there. Realistic positive feedback leading to formation of the observed bars only occurs if the resuspension of sediment due to bore turbulence is included in the model. Also, the offshore root mean square wave height must be larger than 0.5 m and the offshore wave incidence angle larger than 15^{o} (offshore boundary is at 8 m depth), conditions that occur at Duck only 25% of the time. The modelled shape (wavelength, cross-shore extent and crest orientation) and growth rate agree with data, but the model overestimates the migration rates.

1 INTRODUCTION

Patches of several transverse sand bars attached to the shoreline and extending inside the surf zone with an oblique orientation have been observed in open beaches. Alongshore spacings between successive crests range from 20 to 200 m. Several events of formation and evolution of transverse bar patches were observed at Duck beach, USA (Konicki and Holman, 2000), and at Noordwijk beach, the Netherlands (Ribas and Kroon, 2007). These two studies used hourly time-averaged video-images to describe the characteristics of the transverse bars. One to three shore-parallel subtidal bars are very often present in these nearshore zones, sometimes showing a crescentic shape, with undulations at length scales of hundreds of meters (van Enckevort et al., 2004). The transverse bars were most often located inside the trough of the inner bar, attached to the low-tide shoreline, and that is the reason why Konicki and Holman (2000) named them `trough bars'. As an example, figure 1 displays the patch of transverse trough bars observed at Duck on 10 January 1994. Both the percentage of days with patches and the number of bars per patch were significantly lower at Duck, compared with those at Noordwijk. The overall averaged wavelength was 39 m at Noordwijk and 79 m at Duck, and bar crest orientation deviated from the

shore-normal by some 30° and 60°, respectively. Bar patches migrated as a whole at rates up to a few tens of meters per day in the direction of the longshore current. Ribas and Kroon (2007) also correlated the wavelength, crest orientation and migration rate of Noordwijk bars with quantities derived from the hourly wave conditions (measured by an offshore buoy at 18 m water depth). For instance, transverse bar crests deviated from the shore-normal in the up-flow direction (`up-current orientation'). Wave conditions detected in Noordwijk during bar presence were characterized as intermediate waves (root mean square wave height, $H_{rms} \approx 0.75$ m) with large angles of incidence with respect to the shore-normal ($\theta_{off} \approx 50^{o}$ at 18 m depth).

A possible explanation for the formation of transverse bars is based on the concept of morphodynamic self-organization, i.e. the feedbacks between hydrodynamics (waves and currents) and bed evolution (Ribas et al., 2003; Garnier et al., 2006). Here, we will use a model based on linear stability analysis, which has been recently extended to include the dynamics of surface rollers and the corresponding turbulence-induced sediment re-suspension. This extension was essential to successfully explain the formation of transverse bars at Noordwijk (Ribas et al., 2011). Taking surface roller radiation stresses into account also proved to be essential to reproduce accurately the longshore current and wave height profiles measured at Egmond beach, the Netherlands. The aim of the present contribution is to explain under what circumstances transverse bars are formed at Duck beach and what are their main characteristics. Thereby, the model is applied to the bathymetric and offshore wave conditions measured at Duck during the periods when transverse bars were observed by Konicki and Holman (2000). Model results, consisting of the initial shape, and the growth and migration rates of different possible patterns, together with the beach conditions leading to bar formation, are then compared with those observed at Duck.

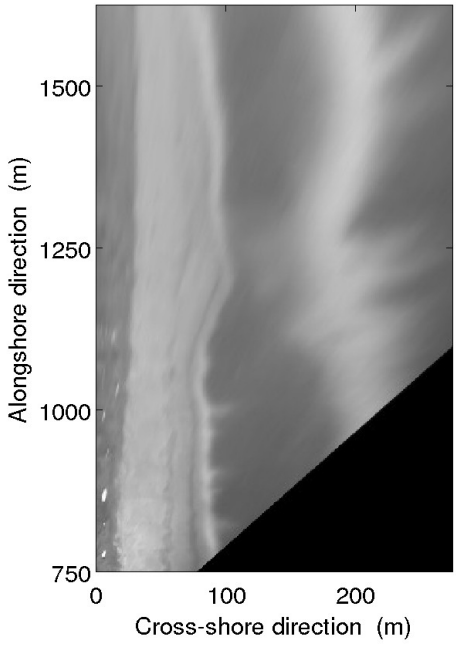

Figure 1 Patch of transverse sand bars observed at Duck beach on 10 January 1994. In this time-averaged planview the white stripes are due to preferential wave breaking on the shallows. A patch of transverse 'trough bars' studied by Konicki and Holman (2000) is visible at x = 100 m and y = [750,1000] m

2 MODEL

2.1 *Equations*

The model is an extension of the model called Morfo60 (Calvete et al., 2005) and describes the feedback between wave and roller dynamics, depth-averaged currents and bed evolution. The y (or x_2) axis is chosen to coincide with the rectilinear shoreline, the x (or x_1) axis points in the seaward direction and the

z axis points upwards. A summary of the model equations are described below and full details can be found in Ribas et al. (2011).

We consider the depth- and time-averaged equations of continuity (1) and momentum (2), and therefore depth-uniform currents, along with a wave dispersion relation (3), a wave energy transformation (4), a roller energy transformation (5), and a bottom evolution equation (6), which follows from conservation of sediment mass. The resulting system of equations is

$$\frac{\partial D}{\partial t}+\frac{\partial}{\partial x_j}\left(Dv_j\right)=0 \qquad j=1,2 \tag{1}$$

$$\frac{\partial v_i}{\partial t}+v_j\frac{\partial v_i}{\partial x_j}=-g\frac{\partial z_s}{\partial x_i}-\frac{1}{\rho D}\frac{\partial}{\partial x_j}\left(S_{ij}^{w}+S_{ij}^{r}-S_{ij}^{t}\right)-\frac{\tau_{bi}}{\rho D} \qquad i,j=1,2 \tag{2}$$

$$\Omega=\sqrt{g\left|\vec{K}\right|\tanh\left(\left|\vec{K}\right|D\right)}+v_jK_j \qquad j=1,2 \tag{3}$$

$$\frac{\partial E}{\partial t}+\frac{\partial}{\partial x_j}\left(\left(v_j+c_{gj}\right)E\right)+S_{jk}^{w}\frac{\partial v_k}{\partial x_j}=-\mathcal{D}_w \qquad i,j=1,2 \tag{4}$$

$$\frac{\partial\left(2E_r\right)}{\partial t}+\frac{\partial}{\partial x_j}\left(2\left(v_j+c_j\right)E_r\right)+S_{jk}^{r}\frac{\partial v_k}{\partial x_j}=-\mathcal{D}_r+\mathcal{D}_w \qquad i,j=1,2 \tag{5}$$

$$(1-p)\frac{\partial z_b}{\partial t}+\frac{\partial q_j}{\partial x_j}=0 \qquad j=1,2 \tag{6}$$

Here, $D = z_s - z_b$ is the water depth, where z_s is the free surface elevation and z_b is the sea bottom level, v_j are the two components of the depth-averaged water velocity, g is gravity, ρ is the water density, τ_{bi} are the bed shear stresses, and S^{w}_{ij}, S^{r}_{ij}, and S^{t}_{ij}, are the wave, roller and turbulence induced radiation stresses, respectively. Furthermore, K_j are the two components of the wave number, Ω is the absolute wave frequency, E and E_r are the wave and roller energy densities, $\mathcal{D}_w$ and $\mathcal{D}_r$ are the wave and roller energy dissipation rates, c_{gj} and c_j are the group and phase velocity components, $p = 0.4$ is the porosity of the bed and q_i are the two components of the wave- and depth-averaged volumetric sediment transport (m^2/s).

The bed shear stresses, τ_{bi} in equation (2), are parameterized following the generalized equation developed by Feddersen et al. (2000), which we have extended to model the effect of a 2-dimensional flow. According to the latter authors, this empirical parameterization adequately represents the shear stresses for the random wave field at Duck. The corresponding drag coefficient c_D is assumed to vary with depth following the Manning-Strickler law (Soulsby 1997), where the bed roughness, k_a, is assumed to be constant in time and space, and its default value, $k_a = 0.035$ m, is within the range of realistic values (Ruessink et al., 2001). The turbulent Reynolds stresses, S^{t}_{ij} in equation (2), are modelled with the standard eddy viscosity approach. The lateral turbulent mixing coefficient is directly linked to the roller energy dissipation rate (the main source of turbulence), $\upsilon_t = M\,(\mathcal{D}_r/\rho)^{1/3}$, where $M = 1$.

Table 1 Default parameter setting, where the offshore wave conditions are the mean values during a transverse bar event at Duck beach from 27 October to 12 November 1994

Parameter	Meaning	Value
k_a	Apparent bed roughness	0.035 m
γ_b	Coefficient of saturation in $\mathcal{D}_w$	0.475
d_{50}	Sediment grain size	0.2 mm
n_{rol}	Roller-induced stirring parameter	40
H^{off}	Offshore rms wave height	0.8 m
θ^{off}	Offshore wave incidence angle	20°
T_p	Peak wave period	7.5 s

Waves are assumed to have a narrow spectrum in frequency and angle. Their heights are supposed to be random and follow the Rayleigh distribution, characterized by the root mean square wave height, H_{rms} (wave energy density being $E = \rho g H^2_{rms}/8$). For brevity, we denote H_{rms} as H from now on. Linear wave theory yields the dispersion relation (3), and expressions for wave properties such as their radiation stresses, S^w_{ij}, the root mean square wave orbital velocity amplitude, u_{rms}, and the two components of the group and phase velocity, c_{gi} and c_i. Steady conditions are assumed, Ω = constant. Applying wavenumber irrotationality, equation (3) is finally rewritten in terms of the wave phase Φ, from which K_i and Ω can be computed. The wave incidence angle with respect to the shore-normal, θ, is computed from K_i and the peak wave period, T_p, is computed from Ω. The energy dissipation rate due to wave breaking, $\mathcal{D}_w$ in equation (4) and (5), is parameterized following Thornton and Guza (1983). This formulation proved to simulate accurate H profiles when compared with field data at Duck. We assume that the fraction of broken waves is $B = 1$, which means that the entire front of the waves is covered with foam, consistent with the derivation of the roller equations. The value used for the saturation ratio of H/D, $\gamma_b = 0.475$, is within the range of recommended values (Thornton and Guza, 1986). Equations (3) and (4) describe the refraction of the waves due to both topography and currents, together with wave breaking. More complex processes in wave propagation, like wave diffraction and reflection, are not accounted for. The energy dissipated by breaking feeds the surface rollers, i.e. the aerated mass of water located on the shoreward face of breaking waves. The wave- and depth-averaged roller energy balance (5) is an extension of the one proposed by Reniers et al. (2004). The radiation stresses due to roller propagation, S^r_{ij}, are computed following Svendsen (1984). The roller energy dissipation rate, $\mathcal{D}_r$, is modelled following Ruessink et al. (2001), with a standard value for the slope of the roller/wave front, $\beta = 0.05$.

A widely accepted formulation for the sediment transport, q_i in equation (6), in nearshore conditions, is that of Soulsby and van Rijn (Soulsby, 1997). Their original expression has been extended to model the effect of a 2-dimensional flow and the preferred downslope transport of the sand,

$$q_i = C_{di}\left(v_i - \Gamma \frac{\partial h'}{\partial x_i}\right) \qquad , \qquad i = 1,2 \qquad , \tag{7}$$

with C_{di} being the depth-integrated sediment concentration, Γ the bedslope coefficient and h' the sea bed perturbations. We have extended Soulsby and van Rijn formula to include the extra contribution to C_{di} due to the stirring of sediment created by the bore induced turbulence, following Reniers et al. (2004),

$$C_{di} = A_s\left(\left(|\vec{v}|^2 + \frac{0.018}{c_D}u^2_{rms} + n_{rol}u^2_{rol}\right)^{0.5} - u_{crit}\right)^{2.4} \qquad , \tag{8}$$

where u_{crit} is the threshold flow intensity for sediment transport, the parameter A_s accounts for the sediment properties, u_{rol} is a representative turbulence velocity of the vortices created after roller energy is dissipated and n_{rol} is a constant parameter. In the original Soulsby van Rijn formula, C_{di} was assumed to be a result of the shear stresses produced in the bottom boundary layer of the wave orbital velocity and the depth-averaged currents (first two terms inside the square root of equation (8)). The Soulsby and van Rijn formula was tested to be accurate in the shoaling domain, at water depths of the order of 5 m (Soulsby, 1997). However, in the inner surf zone (depths < 1 m), where u_{rms} and the longshore current decay, other processes like bore propagation and the created turbulence also produce significant sediment resuspension (Voulgaris and Collins, 2000). In the present study, the third term inside the root square in equation (8) has been added to allow inclusion of this other possible process. We follow Roelvink and Stive (1989), who assumed that this extra u_{rol} was proportional to the dissipation of roller energy,

$$u_{rol} = \left(\frac{\mathcal{D}_r}{\rho}\right)^{1/3}\left(e^{(D/H)} - 1\right)^{-1/2} \qquad . \tag{9}$$

By varying n_{rol} in equation (8) we can change the strength of the sediment stirring due to roller-induced turbulence. A default value $n_{rol} = 40$ is used, which gives reasonable values of C_{di} of some 5 10^{-3} m in the inner surf zone. The original Soulsby van Rijn C_{di} is obtained for $n_{rol} = 0$. The Manning-Strickler law is again assumed for the drag coefficient c_D and the full expressions for u_{crit} and A_s are given in Soulsby

(1997).

The bedslope term in equation (7) accounts for the tendency of the system to smooth out the sea bed perturbations, *h'*, if they do not cause positive feedback into the flow. The coefficient Γ has also been extended to include the effect of the surface rollers,

$$\Gamma = \gamma\left(\left(|\vec{v}|^2 + \frac{0.018}{c_D}u_{rms}^2 + n_{rol}u_{rol}^2\right)^{0.5} - u_{crit}\right)^{2.4} \quad , \qquad (10)$$

with $\gamma = 0.5$ being the bedslope parameter. The value used yields bedslope coefficients similar in magnitude to those of the original Soulsby and van Rijn formulation (Soulsby, 1997)

The fluid velocities are imposed to vanish at both the coastline and the offshore boundary, where we also assume a fixed bed level. Also, the free surface elevation and E_r are assumed to vanish at the offshore boundary, where wave conditions are prescribed (H^{off}, θ^{off} and T_p). The offshore boundary is at 1000 m from the shoreline, the location of the buoy in front of Duck beach (8 m water depth).

2.2 *Methods*

The equations (1)-(6), which govern this morphodynamic system, together with the parameterizations used, define a closed dynamical system for the variables v_1, v_2, z_s, E, E_r, Φ and z_b. The stability analysis approach to the formation of bars by self-organization starts by defining a steady and alongshore uniform basic state (i.e., without longshore rhythmic topography). In this study, we used a reference profile, $z_b^o(x)$, measured at Duck, which showed one well-developed shore-parallel bar. The modelled basic state is characterized by the presence of a longshore current, $v^o{}_1 = 0$ and $v^o{}_2 = V^o(x)$, and an elevation of the mean sea level, $z_s^o = z_s^o(x)$ (figure 2). This basic state only represents a morphodynamic equilibrium if the net cross-shore sediment flux vanishes. The superscript ^{o} denotes the basic state variables.

Once the basic state has been computed, linear stability analysis can be applied in a standard way. A small perturbation, assumed to be periodic in time and in the alongshore coordinate, is added to this state,

$$(v_1, v_2, z_s, E, E_r, \Phi, z_b) = (0, V^o, z_s^o, E^o, E_r^o, \Phi^o, z_b^o) + \Re e\left\{e^{(\omega t + i\kappa y)}(u, v, \eta, e, e_r, \phi, h)\right\} \quad . \qquad (11)$$

where κ is the alongshore wavenumber and ω a complex growth rate. By inserting equation (11) in the governing equations and linearizing with respect to the perturbations, we arrive at an eigenproblem. For each κ, different eigenvalues ω exist, which characterize the different growing modes, and the complex eigenfunctions are $(u(x), v(x), \eta(x), e(x), e_r(x), \phi(x), h(x))$. The growth rate of the emerging bars is given by $\Omega = \mathcal{Re}(\omega)$, so that $\Omega > 0$ means growth. In case of an unstable basic state, solutions with $\Omega > 0$ are found and the growth rate curves show these positive Ω for different values of κ. Starting from arbitrary initial conditions, the dynamics after some time will be dominated by the mode with largest growth rate, which is called Fastest Growing Mode (FGM). Its *e*-folding growth time is given by $T_g = 1/\Omega$ and its migration speed by $c = -\mathcal{Im}(\omega)/\kappa$. The alongshore wavelength of the corresponding bar patch is $\lambda = 2\pi/\kappa$ and the shape of the final topography and the associated quantities are given by equation (11).

3 RESULTS

3.1 *Default case study*

The default case study (table 1) is based on one of the best developed transverse bar events described by Konicki and Holman (2000), the one occurring from 27 October to 12 November 1994. Several bathymetric measurements are available during that period because the Duck94 nearshore experiment was being performed. The profile measured on 26 October 1994 at y = 900 m has been chosen as reference profile because it was measured one day before the event started and at the alongshore location where the transverse bars were subsequently observed. The wave conditions measured at the 8 m depth buoy were used, because it was the only directional buoy during the study period. The default wave conditions were the mean values during the whole event duration. The resulting basic state solution, displayed in figure 2, shows the presence of strong peaks of the longshore current and of the depth-integrated sediment

concentration at the inner surf zone (0<x<50 m), were most of the wave and roller energy dissipates.

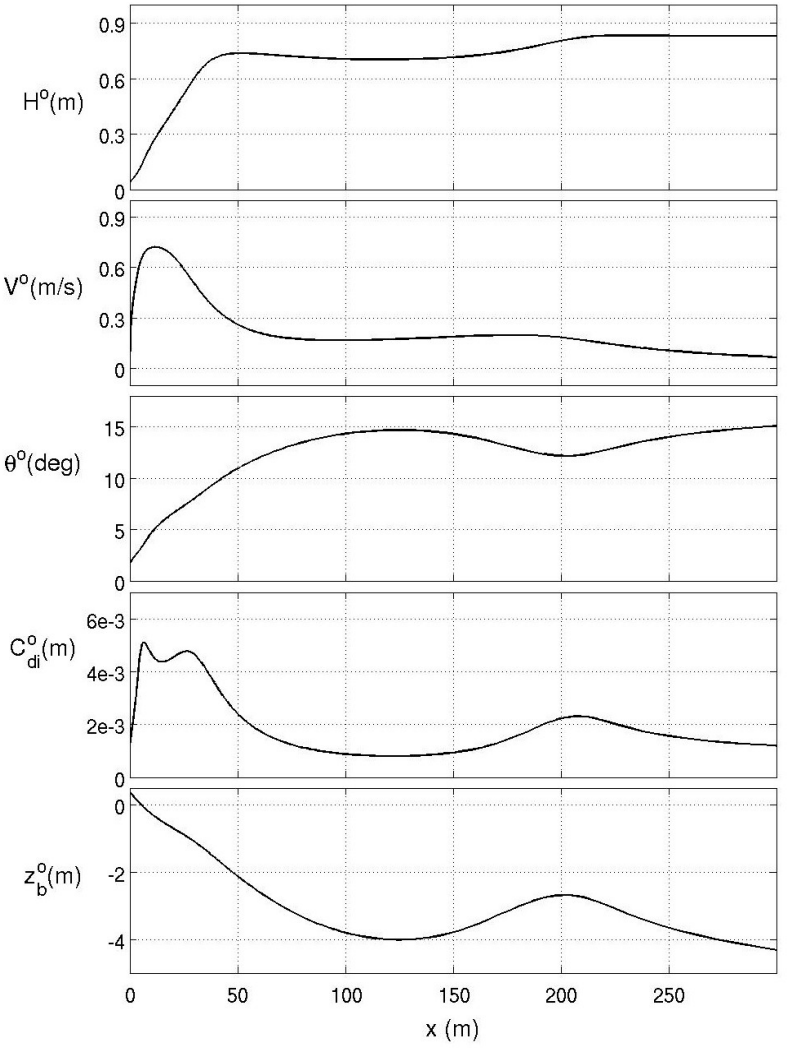

Figure 2 Basic state solution obtained for the default case study. Panels show, from top to bottom: rms wave height, longshore current, wave incidence angle, depth-integrated sediment concentration and bed level

The result of the linear stability analysis obtained for the default parameter setting is shown in figure 3. The growth rate curve shows a clear maximum for κ = 0.082 m^{-1}, which corresponds to a wavelength λ = 77 m, an *e*-folding growth time T_g = 13 h and a migration rate c = 87 m/d. The middle panel in figure 3 displays the shape of the topographic perturbation corresponding to this fastest growing mode. The small arrows indicate the main trend in the deviations of the longshore current due to the hydrodynamic circulation induced by the growing bars. As can be seen, the solution consists of a patch of up-current oriented bars, whose crests deviate 46 ^{o} from the shore-normal, with current perturbations deflecting offshore over their crests (the reference longshore current is directed from left to right in topographic panels). The bars extend seaward up to 53 m from the shoreline. In order to visualize the final shape of the bottom, the reference profile, z_b^o, should be added to the topographic perturbations shown in figure 3. The same applies to the flow: the longshore current, V^o, should be added to the perturbations of the velocity to obtain the total flow.

The lower panel in figure 3 shows the shape of the topographic perturbation corresponding to the maximum of the secondary mode obtained for smaller wave numbers. The solution is a crescentic bar with a wavelength λ = 790 m, an *e*-folding growth time T_g = 130 h and a migration rate c = 38 m/d. This study focuses on transverse bars and, therefore, the crescentic bar solution will not be discussed longer.

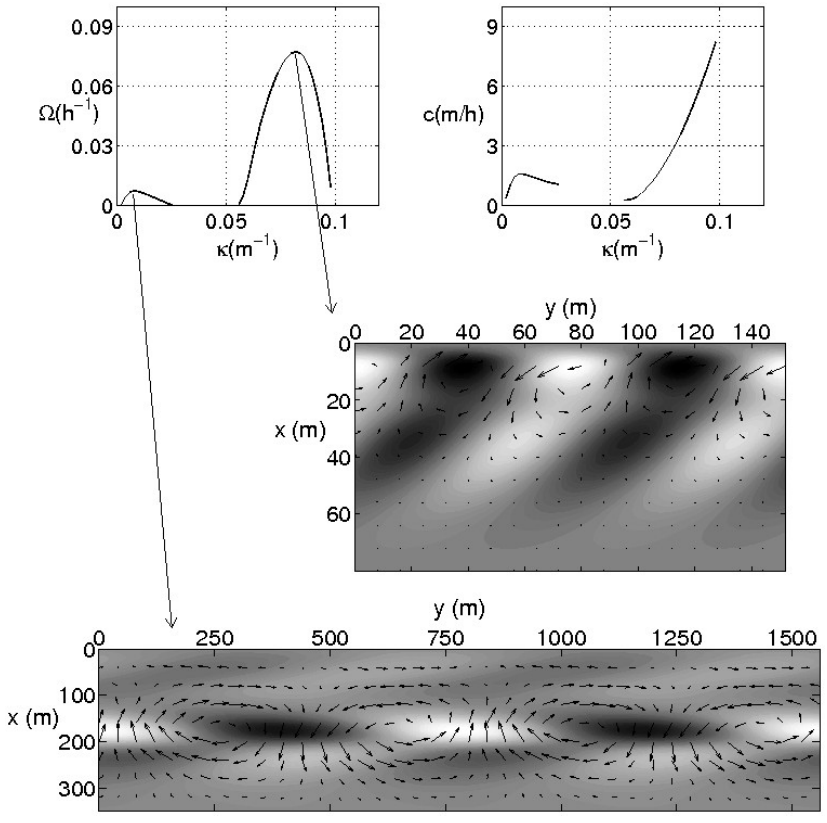

Figure 3 Linear stability analysis solution obtained for the default case study. Growth and migration rate curves (upper panels) and topographic and current perturbations corresponding to the transverse bar solution (middle) and to the crescentic bar solution (lower). In the topographic plots, white (dark) areas indicate crests (troughs). Waves approach the coast from the bottom left corner, so the equilibrium longshore current is directed from left to right, and small arrows indicate the current perturbations

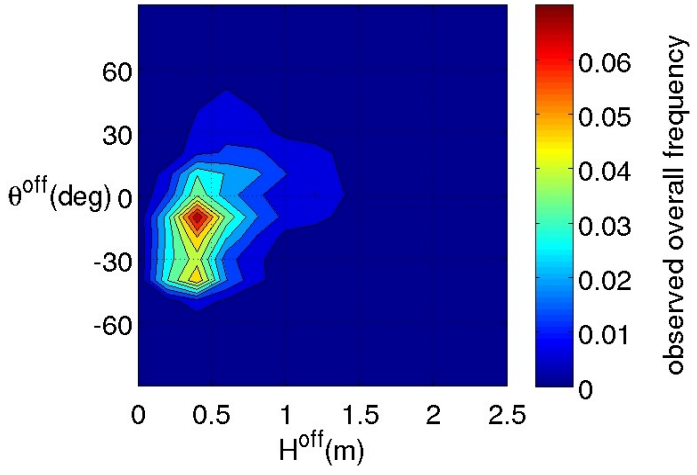

Figure 4 Frequency of occurrence of H^{off} and θ^{off} observed at the 8 m depth buoy in front of Duck beach from 1987 to 1996, the full time period studied by Konicki and Holman (2000)

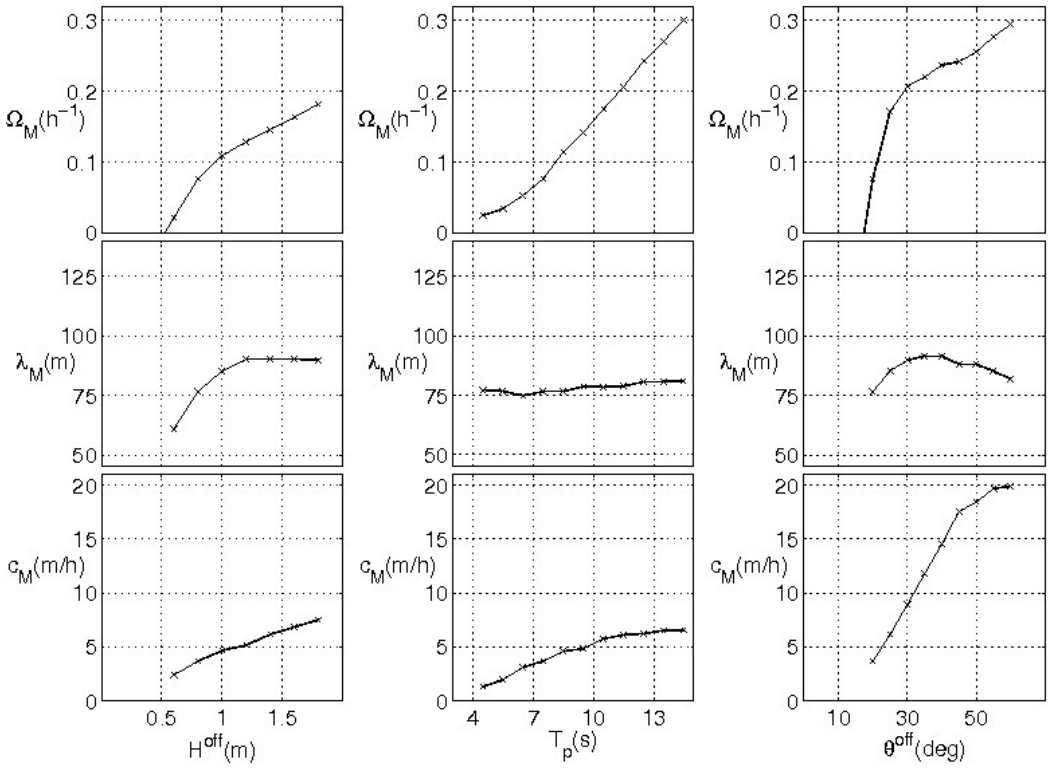

Figure 5 Characteristics of the transverse bars obtained for different offshore wave conditions. Growth rate (upper panels), wavelength (middle panels) and migration rate (lower panels) are shown for different offshore rms wave height (left panels), peak wave period (central panels) and offshore angle of wave incidence (right panels)

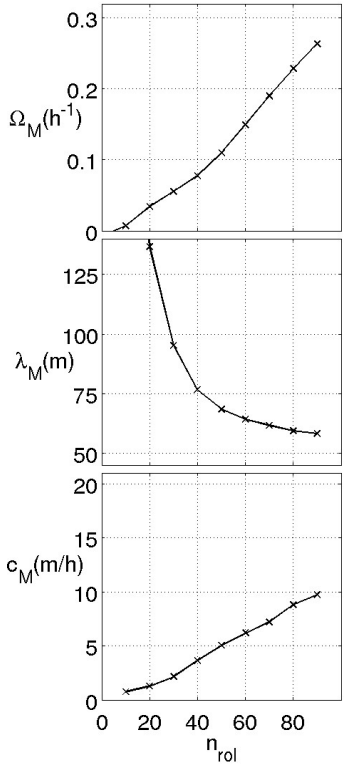

Figure 6 Growth rate (upper panel), wavelength (middle panel) and migration rate (lower panel) are shown for different values of the roller-induced stirring parameter

3.2 *Varying the offshore wave conditions and the roller-induced stirring parameter*

Sensitivity of bar characteristics to varying the offshore wave conditions has been subsequently checked. The range of values observed at the 8 m depth buoy from 1987 to 1996 (the full time period studied by Konicki and Holman (2000), shown in figure 4) is applied as model input. Each wave parameter (H^{off}, T_p and θ^{off}) has been varied keeping the other two equal to their default values. In general, growth rate increases when H^{off}, T_p and θ^{off} become larger, and only if $H^{off} > 0.5$ m and $\theta^{off} > 15^o$ transverse bars are formed (upper panels of figure 5). The wavelength is less dependent on wave conditions, its value ranging from 60 to 90 m (middle panels of figure 5). The migration rate increases with increasing H^{off} and T_p, but it becomes especially large in case $\theta^{off} > 30^o$ (lower panels of figure 5). Bar crest orientation also increases when θ^{off} is enlarged, with the subsequent decrease in cross-shore extent of the bars.

The value of the turbulence-induced stirring parameter, n_{rol}, has also been varied, given the limited experimental knowledge of this phenomenon (figure 6). Transverse bars are not formed if the value of this parameter is set to zero, which means that the formation of these bars can not be modelled with the original Soulsby van Rijn sediment transport formula (equation 8 with $n_{rol} = 0$). In case $n_{rol} > 10$, when its value increases the growth and migration rates of the bars become larger and their wavelengths decrease.

Table 2 Comparison between model results and field observations at Duck.

	Wavelength (m)	**Cross-shore extent (m)**	**Crest orientation**	**Migration rate (m/d)**
Model	58-137	36-63	43^o-63^o	0-400
Data	12-179	10-50	$58^o \pm 17^o$	0-40

4 DISCUSSION

4.1 *Comparison with observations*

The model results turn out to be in good agreement with observations. The modelled wavelength of the maximum growing solution in the default case, consisting of patches of transverse bars with wavelengths of 77 m (figure 3), is similar to the observed bar patches. The wavelength reported by Konicki and Holman (2000) for the event observed from 27 October to 12 November 1994 was 66 m. Table 2 shows that this comparison is also positive if all the data collected at Duck is compared with the model results obtained when varying the wave conditions with the values measured during the time period studied by Konicki and Holman (2000). The similarities are especially remarkable in the magnitudes quantifying the bar patch shape: wavelength, cross-shore extent and crest orientation. Regarding crest orientation, the averaged value observed in the field was 58^o and the standard deviation 17^o, which is in good agreement with modelled orientations, varying from 43^o to 63^o. Notice that Konicki and Holman (2000) did not relate crest orientation with wave incidence angle; hence the model result that bars are up-current oriented can not be verified with the available data. Measuring the growth rate of the bars observed in the field was not possible due to the nature of the detection technique (video imaging). However, the order of magnitude of the modelled growth time (half a day) is consistent with the observations. Finally, note that modelled migration rates are one order of magnitude larger than the daily averaged rates detected in the field (a few hundreds of m/day and a few tens of m/d, respectively). However, realize that the reported daily-averaged values are very often smaller than the instantaneous migration rates.

The model results yield clues which explain why transverse bar patches at Duck occurred less frequently and had a smaller number of bars per patch than at Noordwijk (Ribas and Kroon, 2007). According to our model, transverse bars can grow only if $H^{off} > 0.5$ m and $\theta^{off} > 15^o$ (figure 5), but those conditions do not occur often at Duck, a site with an important amount of shore-normal waves and low wave heights (figure 4). The percentage of time during which the wave conditions at the 8 m depth buoy verified the threshold conditions ($H^{off} > 0.5$ m and $\theta^{off} > 15^o$) was only 25%. This percentage was calculated using the wave conditions from 1987 to 1996 (the data shown in figure 4), the full time period studied by Konicki and Holman (2000). Realize that this is not a sufficient but only a necessary condition for bar presence. Also, wave conditions must be regular during at least one day and bathymetric characteristics can play an

important role (Ribas and Kroon, 2007), which has not been studied in the present contribution. In any case, the percentage of time with wave conditions leading to bar formation at Noordwijk is significantly larger, because the Dutch coast is nearly always subject to oblique wave incidence (Ribas and Kroon, 2007).

4.2 *Physical mechanism*

The similarities between the model results and Duck bars indicate that the physical mechanism based on a feedback between waves, rollers, currents and bed evolution, first described in Ribas et al. (2003), could explain the development of transverse bars in this beach. The growing bars modify locally the longshore current, which veers offshore over the crests of up-current oriented bars (middle panel of figure 3). Positive feedback occurs because the depth-averaged sediment concentration, $C_{da} = C_{di}/D$, (where C_{di} is the depth-integrated concentration and D is the water depth) decreases seaward across the inner surf zone, thereby creating a convergence of sediment transport in the offshore directed flows. Including the roller-induced turbulence stirring is essential to explain this cross-shore distribution of C_{da} leading to bar formation. If this phenomenon is neglected, as done in the standard sediment transport formulas used in morphodynamic models, the obtained C_{da} profile can not produce transverse bar formation.

There is another aspect of roller dynamics that plays a damping role in transverse bar formation. The roller-induced radiation stresses in the momentum equation (2) create hydrodynamic forces that act mostly against the formation of the needed offshore directed current perturbations over the bar crests. Indeed, if the roller radiation stresses are neglected in the momentum equations of our model, the formation of up-current oriented bars is predicted to occur with quite a larger growth rate. The main reason for this behaviour is that roller energy is larger over the crests of the growing bars (because wave breaking increases at the shallows) and then decreases in the shoreward direction, providing a strong gradient in the cross-shore component of the roller radiation stresses and the corresponding shoreward directed force. This effect is stronger as wave incidence angle is smaller and it can even inhibit bar formation if the angle is below the threshold value.

5 CONCLUSIONS

A self-organization morphodynamic model has been able to explain the formation of transverse bars at Duck beach, USA. The model has been applied to the conditions measured at Duck during the period when transverse bars were observed by Konicki and Holman (2000). The bathymetric profiles of the alongshore positions where bars were observed and the wave conditions measured at a buoy located in front of the beach at 8 m depth have been used. Modelled bar characteristics have then been compared with the transverse bar characteristics observed at Duck.

The default case study is based on the beach conditions measured at Duck from 26 October to 17 November 1994, when a patch of transverse bars was observed. Wave conditions are subsequently varied following those measured during the full time period studied by Konicki and Holman (2000). The obtained fastest growing solution consists of a patch of up-current oriented bars, which are similar to the observed ones. The modelled wavelength (58-137 m), cross-shore extent (36-63 m) and crest orientation (43^o-63^o) are in good agreement with Duck data. The modelled bars are up-current oriented because their seaward end is shifted up-flow with respect to the longshore current. However, this specific model outcome can not be compared with the observations at Duck because Konicki and Holman (2000) did not relate bar orientation with wave conditions. The modelled growth rate (of the order of half a day) is also realistic. However, modelled migration speeds (a few hundreds of m/day) are higher than those measured in the field.

Sensitivity of bar characteristics to the wave conditions and other model parameters has also provided information about the circumstances leading to transverse bars formation. An essential condition is that both the wave incidence angle and the wave height are larger than a certain threshold, conditions that only occur at Duck 25% of the time. Another important result is that bar can only grow if the roller-induced turbulence stirring is taken into account. The rollers create turbulent bores that can lead to significant sediment resuspension in the inner surf zone. This gives a cross-shore distribution of the depth-averaged volumetric sediment concentration that can explain the formation of up-current bars at Duck site.

6 ACKNOWLEDGEMENTS

Funding from the Spanish research project `Modelización y monitorización integradas en morfodinámica de playas naturales y regeneradas' (contract CTM2009-11892) is acknowledged. Duck Data are provided by the Field Research Facility, Field Data Collections and Analysis Branch, US Army Corps of Engineers, Duck, North Carolina. We thank Dr. Nathaniel Plant for the image in figure 1.

REFERENCES

Calvete D., Dodd N., Falqués A. and van Leeuwen S.M. 2005, Morphological development of rip channel systems: Normal and near normal wave incidence. Journal of Geophysical Research, Vol.110, C10006, doi:10.1029/2004JC002803.

Feddersen F., Guza R. T., Elgar S. and Herbers T. H. C. 2000, Velocity moments in alongshore bottom stress parameterizations. Journal of Geophysical Research, Vol.105, N.C4, pp. 8673–8686.

Garnier R., Calvete D., Falqués A. and Caballeria M. 2006, Generation and nonlinear evolution of shore-oblique/transverse sand bars. Journal of Fluid Mechanics, Vol.567, pp. 327–360.

Konicki K. M. and Holman R. A. 2000, The statistics and kinematics of transverse bars on an open coast. Marine Geology, Vol.169, pp. 69–101.

Reniers A. J. M. H., Roelvink J. A. and Thornton E. B. 2004, Morphodynamic modeling of an embayed beach under wave group forcing. Journal of Geophysical Research, Vol.109, C01030, doi:10.1029/2002JC001586.

Ribas F., Falqués A. and Montoto A. 2003, Nearshore oblique sand bars. Journal of Geophysical Research, Vol.108, C43119, doi:10.1029/2001JC000985.

Ribas F. and Kroon A. 2007, Characteristics and dynamics of surfzone transverse finger bars. Journal of Geophysical Research, Vol.112, F03028, doi:10.1029/2006JF000685.

Ribas F., de Swart H. E., Calvete D. and Falqués A. 2011, Modelling waves, currents and sandbars on natural beaches: the effect of surface rollers. Journal of Marine Systems 88, pp. 90-101, doi: 10.1016/j.jmarsys.2011.02.016.

Roelvink J. A. and Stive M. J. F. 1989, Bar-generating cross-shore flow mechanisms on a beach. Journal of Geophysical Research, Vol.94, N.C4, pp. 4785–4800.

Ruessink B. G., Miles J. R, Feddersen F., Guza R. T. and Elgar S. 2001, Modeling the alongshore current on barred beaches. Journal of Geophysical Research, Vol.106, N.C10, pp. 22451–22463.

Soulsby R. L. 1997, Dynamics of Marine Sands. London, U.K.: Thomas Telford.

Thornton E. B., and Guza, R. T. 1983, Transformation of wave height distribution, Journal of Geophysical Research, Vol.88, N.C10, pp. 5925–5938.

Thornton E. B., and Guza, R. T. 1986, Surf zone longshore currents and random waves: field data and models, Journal of Physical Oceanography, Vol.16, pp. 1165–1178.

Svendsen I. A. 1984, Wave heights and setup in the surf zone. Coastal Engineering, Vol.8, pp. 303–329.

van Enckevort I. M. J., Ruessink B.G., Coco G., Suzuki K, Turner I.L., Plant N.G., and Holman R.A., 2004, Observations of nearshore crescentic sandbars. Journal of Geophysical Research, Vol.109, C06028, doi:10.1029/2003JC002214.

Voulgaris G., and Collins M. B. 2000, Sediment resuspension on beaches: response to breaking waves. Marine Geology, Vol.167, pp. 167–187.